Journal of Alloys and Compounds 471 (2009) 502–506

Contents lists available at ScienceDirect

Journal of Alloys and Compounds

journal homepage: www.elsevier.com/locate/jallcom

Oxidation of ZrB_2 powder in the temperature range of 650–800 °C

Wei-Ming Guo, Guo-Jun Zhang*, Yan-Mei Kan, Pei-Ling Wang

State Key Laboratory of High Performance Ceramics and Superfine Microstructures, Shanghai Institute of Ceramics, Shanghai 200050, China

ARTICLE INFO

Article history:
Received 23 February 2008
Received in revised form 1 April 2008
Accepted 3 April 2008
Available online 19 May 2008

Keywords:
Kinetics
Microstructure
Oxidation

ABSTRACT

The isothermal oxidation of ZrB_2 powder was carried out in the range of 650–800 °C in a flowing air using thermogravimetric analysis (TGA). The evolution of the phase characterization and morphology of ZrB_2 powder oxidized at 700 °C for varying durations was studied by X-ray diffraction (XRD) and scanning electron microscopy (SEM), respectively. The excellent fit of TG curves by multiple-law model suggests that the oxidation of ZrB_2 powder in air follows para-linear kinetics, and based on the fitted results, oxidation mechanisms can also be obtained. The reaction product of ZrB_2 powder with oxygen is metastable tetragonal ZrO_2 at 700 °C, and the tetragonal phase transforms to the monoclinic phase with oxidation. The oxidation of ZrB_2 powder is associated with surface microcrack formation, which is attributed to volume expansion resulting from oxidation of ZrB_2 to tetragonal ZrO_2 and tetragonal-to-monoclinic phase transformation of ZrO_2. In the last stage of oxidation, each ZrB_2 particle breaks into fragments.

1. Introduction

Many transition-metal diborides have attracted considerable attention owing to the excellent combination of physicochemical properties such as high melting temperature, high hardness, and high thermal conductivity. ZrB_2 is one of these diborides and a candidate for use in the thermal protection systems and scramjet engine components for hypersonic flight vehicles, as well as high temperature electrodes, molten metal containment systems, and incinerators, because of its good resistance to ablation at high temperatures and thermal-shock resistance in addition to the attractive aforementioned properties [1,2].

When ZrB_2 is exposed to oxidizing environments at high temperatures, it oxidizes, which will degrade its properties. Thus, a large number of studies on oxidation of ZrB_2 and its composites in air have been carried out in order to better understand the oxidation mechanisms and enhance oxidation resistance [3–12]. The reaction of ZrB_2 with O_2 is as follows:

$$ZrB_2 + \tfrac{5}{2}O_2(g) \rightarrow ZrO_2 + B_2O_3(l) \qquad (1)$$

B_2O_3 is known to have a low melting point of 450 °C and high vapor pressure, so it readily vaporizes at high temperatures.

$$B_2O_3\,(l) \rightarrow B_2O_3\,(g) \qquad (2)$$

Researchers have studied the products resulting from the oxidation of ZrB_2, and discovered that the oxide scale is composed of an external glassy B_2O_3 layer and an underlying porous ZrO_2 layer filled with B_2O_3. The glassy B_2O_3 film acts as an effective barrier against oxygen diffusion, and the porous ZrO_2 layer does not offer effective protection. At temperatures below 1100 °C, a parabolic behavior was reported for the oxidation of ZrB_2 due to the presence of a continuous layer of B_2O_3 [3,8–10]. B_2O_3 rapidly vaporizes at temperatures above 1100 °C, thus reducing the effectiveness of the diffusion barrier. Para-linear kinetics have been observed in the temperature range of 1100–1400 °C [4,8–10]. Because the removal of the B_2O_3 layer above 1400 °C leaves behind a porous ZrO_2 scale, ZrB_2 exhibits rapid linear oxidation kinetics at these temperatures [9,10].

It has been almost 50 years since researchers started to explore the oxidation of ZrB_2. However, previous investigations have mainly focused on the oxidation of bulk materials, oxidation mechanisms of ZrB_2 powder as well as phase composition and microstructures that evolve during oxidation have not been studied in detail. In this paper, the oxidation behavior of ZrB_2 powder from 650 to 800 °C in air was investigated. Firstly, the isothermal oxidation kinetics and mechanisms were studied by multiple-law model. Then the evolution of phase characterization and morphology of the samples before and after oxidation was described.

2. Experimental

The ZrB_2 powder employed in this study was a commercial product (Kojundo Chemical Laboratory Co. Ltd, Saitama, Japan). The surface area of the sample was $0.3042\,m^2/g$, as measured by the BET method. Oxidation tests were carried out by a Netzsch STA449C simultaneous thermal analyzer under isothermal conditions. The samples were heated to the desired temperature (650, 700, 750, and 800 °C) for the isothermal oxidation in flowing nitrogen (99.99%, 50 ml/min). The fast heating stage with a heating rate of 50 °C/min prior to the isothermal period was applied

---

* Corresponding author. Tel.: +86 21 52411080; fax: +86 21 52413122.
E-mail address: gjzhang@mail.sic.ac.cn (G.-J. Zhang).

0925-8388/$ – see front matter © 2008 Elsevier B.V. All rights reserved.
doi:10.1016/j.jallcom.2008.04.006

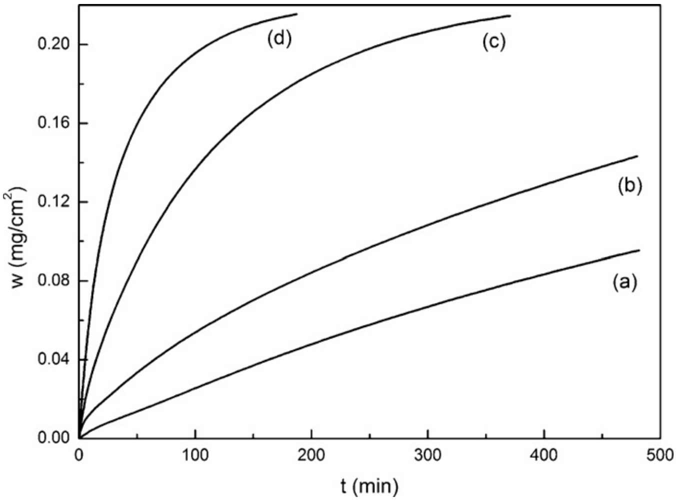

Fig. 1. Thermogravimetric curves of ZrB_2 powder oxidized in air at different temperatures: (a) 650 °C; (b) 700 °C; (c) 750 °C; and (d) 800 °C.

to minimize oxidation effects before reaching the target temperatures. When the desired temperature was reached, the sample was held at that temperature for about 5 min before the gas was switched from nitrogen to air. Roughly 60 mg of ZrB_2 powder was placed into an alumina crucible and oxidized in flowing air (50 ml/min). Due to the low oxidation temperatures, no obvious interaction between the sample and the crucible was observed. Phase composition and morphology of the samples before and after oxidation were studied by X-ray diffraction (XRD) with Cu Kα radiation and scanning electron microscopy (SEM), respectively.

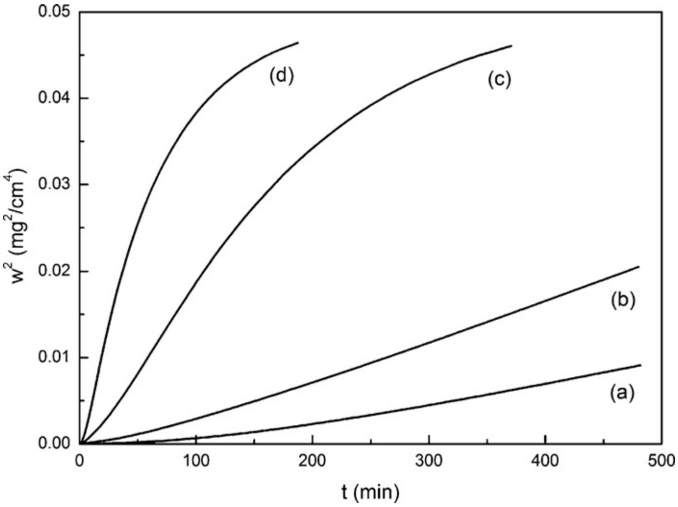

Fig. 2. Square of mass gain versus time for ZrB_2 powder oxidized in air at different temperatures: (a) 650 °C; (b) 700 °C; (c) 750 °C; and (d) 800 °C.

3. Results and discussion

3.1. Oxidation kinetics and mechanisms

TG curves of ZrB_2 powder oxidized in air at 650–800 °C are shown in Fig. 1, where w is the mass gain per unit surface area and

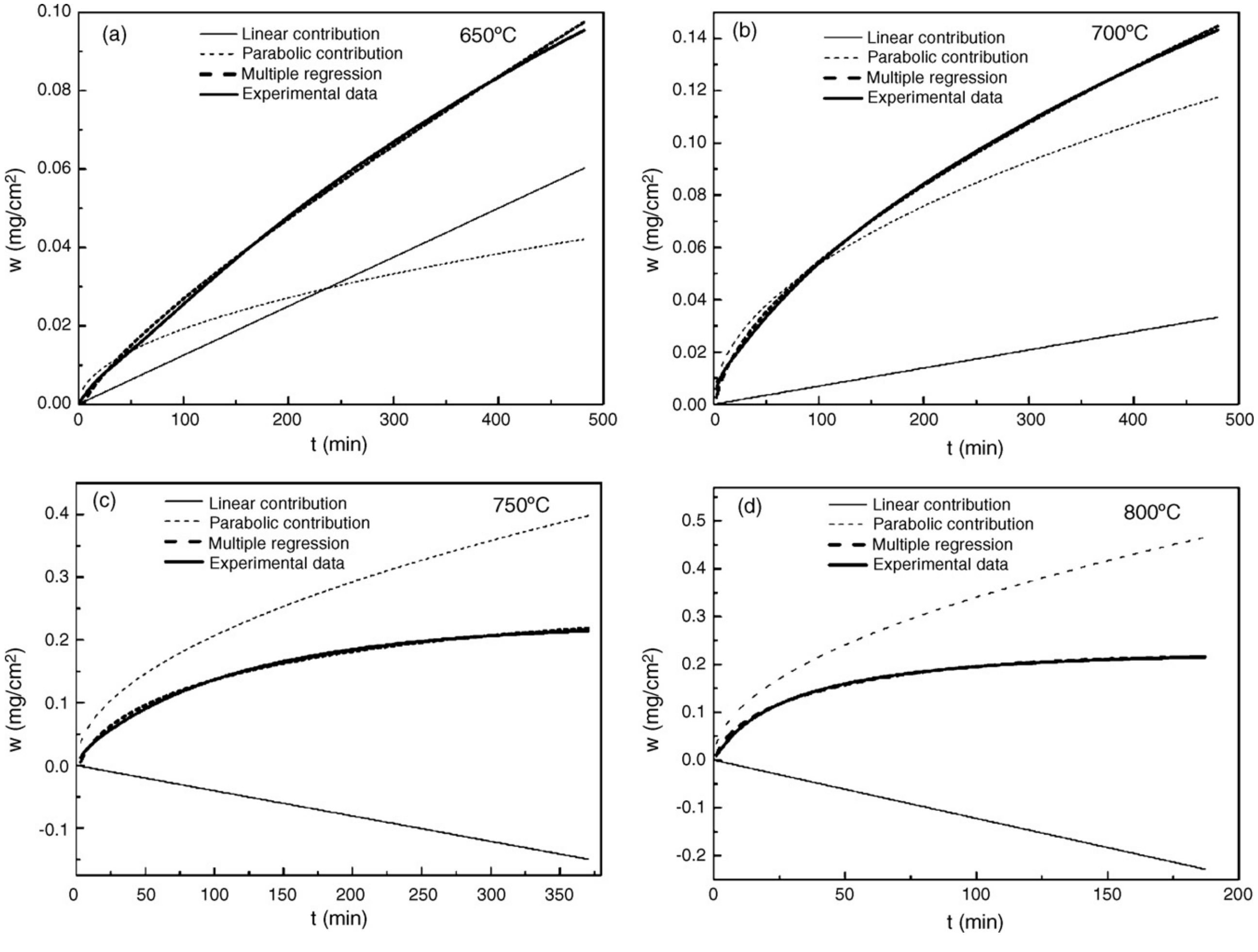

Fig. 3. Multiple-law modeling of TG curves of ZrB_2 powder oxidized in air at different temperatures: (a) 650 °C; (b) 700 °C; (c) 750 °C; and (d) 800 °C.

t is oxidation time. With increasing temperature, it is obvious that the weight gain increases at identical time. It can be seen that the TG curve approaches linear behavior for 650 °C, whereas TG curves clearly show deviation from linear behavior with the increase of temperature.

Fig. 2 presents the square of mass gain per unit surface area as a function of oxidation time for ZrB_2 powder. It is found that the square of mass gain per unit surface area is a nonlinear function of oxidation time, which indicates that oxidation of ZrB_2 powder deviates from parabolic kinetics. Therefore, a simple parabolic law is unable to describe the kinetic behavior. In order to give a complete analytical description, the TG curves were fitted according to a multiple-law model including a linear and parabolic term, developed by Nickel [13]. The mass change per unit area w is expressed as a function of time, according to the following equation:

$$w = A + K_{\text{lin}} t + K_{\text{par}} \sqrt{t} \tag{3}$$

where A is a constant, K_{lin} is linear rate constant and K_{par} is parabolic rate constant. The fit allows for the quantification of the individual contributions of the multiple-law model and accounts for para-linear kinetics. Using multiple linear-regression analysis, multiple-law modeling of TG curves of ZrB_2 powder oxidized in air at different temperatures was performed, with the results illustrated in Fig. 3. The K parameters and R^2 values corresponding to each fitting curve are reported in Table 1. The excellent fit of the solutions confirms that oxidation of ZrB_2 powder follows para-linear kinetics in such a temperature range ($R^2 > 0.99$).

As seen in Fig. 3, the dominating term is the parabolic one in the range of 650–800 °C, accounting for oxygen diffusion in oxide scale. From 650 to 700 °C, the linear term is positive, which is related to mass gain due to chemical reaction between ZrB_2 and O_2 at the diboride–oxide interfaces. In the range of 750–800 °C, the linear term is negative, which is associated with mass loss due to vaporization of B_2O_3. It can therefore be inferred that oxidation of ZrB_2 powder in air is governed by oxygen diffusion and chemical reaction at 650–700 °C, but controlled by oxygen diffusion and the evaporation of B_2O_3 at 750–800 °C.

Even though the vapor pressure of B_2O_3 may be low in the temperature range of 750–800 °C, oxidation kinetics revealed that the evaporation of B_2O_3 should not be neglected during the oxidation of ZrB_2 powder. This deduction can be also supported by the study on oxidation of AlN–SiC–ZrB_2 composites reported by Brach et al. [14]. In the range 700–900 °C, Brach et al. [14] indicated the oxidation of AlN–SiC–ZrB_2 composites followed mixed para-linear kinetics, where the linear term was negative, accounting for mass loss due to vaporization of B_2O_3.

3.2. Phase characterization and morphology of the oxidized samples

Fig. 4 shows the XRD patterns of ZrB_2 powder oxidized at 700 °C for varying durations. Before the exposure, only ZrB_2 peaks are detected as shown in Fig. 4a. In the initial stage of oxidation, tetragonal ZrO_2 peaks appear (Fig. 4b). With increasing oxidation time, monoclinic ZrO_2 peaks also appear, while intensities of ZrB_2 peaks simultaneously decrease, as shown in Fig. 4c. When oxidation time is increased to 15 h at 700 °C, the XRD patterns show monoclinic ZrO_2 as a major phase, a minor phase of tetragonal ZrO_2, and the disappearance of the ZrB_2 phase (Fig. 4d).

Table 1
Kinetic parameters of the oxidation fitting curve, relatively to parabolic and linear contributions, and R^2 (fit goodness) values.

Oxidation temperature (°C)	K_{par} (mg cm^{-2} min$^{-0.5}$)	K_{lin} (mg cm^{-2} min^{-1})	R^2
650	0.00192	0.00013	0.99852
700	0.00536	0.00007	0.99947
750	0.02068	−0.00040	0.99744
800	0.03405	−0.00122	0.99886

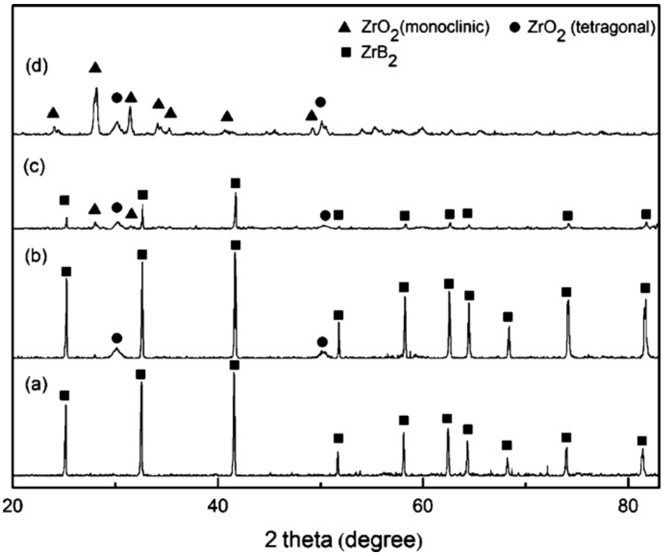

Fig. 4. X-ray diffraction patterns of ZrB_2 powder oxidized at 700 °C for varying durations: (a) no oxidation; (b) 0.5 h; (c) 4 h; and (d) 15 h.

Generally, the stable polymorph of zirconia at room temperature and atmospheric pressure is monoclinic, which transforms at 1170 °C to tetragonal and then at 2370 °C to cubic structure. Previous researchers [15] have investigated the effect of the crystallite size on the phase transformation and pointed out that the phase transformation was closely related to the growth of the crystallite size. When the particle size reaches nano-scale, a metastable tetragonal ZrO_2 can also exist at room temperature, which is so-called nanosize effect of particle phase [16]. So, the reaction of ZrB_2 powder with oxygen can generate metastable tetragonal ZrO_2 instead of stable monoclinic phase at 700 °C. Broad ZrO_2 peaks also validate this deduction in Fig. 4b. However, the tetragonal crystallites grow during annealing. Upon reaching a critical diameter, the tetragonal phase transforms immediately to the monoclinic phase. Therefore, monoclinic ZrO_2 peaks appear with oxidation. The increase of holding time will induce more phase transform of ZrO_2, and as a result, the oxidized samples after 15 h contains major monoclinic ZrO_2 phase with minor tetragonal ZrO_2 phase.

Morphology changes occurring to the ZrB_2 powder as a result of oxidation were examined using SEM. Fig. 5 is a montage of SEM images illustrating the progression of oxidation at 700 °C. The as-received ZrB_2 powder consists of irregularly sized particles with mainly columnar shape, as shown in Fig. 5a. The first visible evidence of appreciable oxidation of the samples is the appearance of circumferential microcracks at the edge of the ends of a number of cylinders, for example, on the arrow sites in Fig. 5b. At the beginning of oxidation, the particles keep their original shape, while the surfaces become rough. With further oxidation, microcracks at the surface of the oxide layers running parallel to the central axes of the cylinders are also observed (indicated by arrows in Fig. 5c). At the same time, the oxide scale at the ends of certain columnar particles flake off. After 15 h, every ZrB_2 particle has broken into several fragments (Fig. 5d).

It is assumed that oxidation products have theoretical density. Therefore, the oxidation from ZrB_2 to tetragonal ZrO_2 is accompanied by 9% volume expansion, based on the densities of 6.09 and

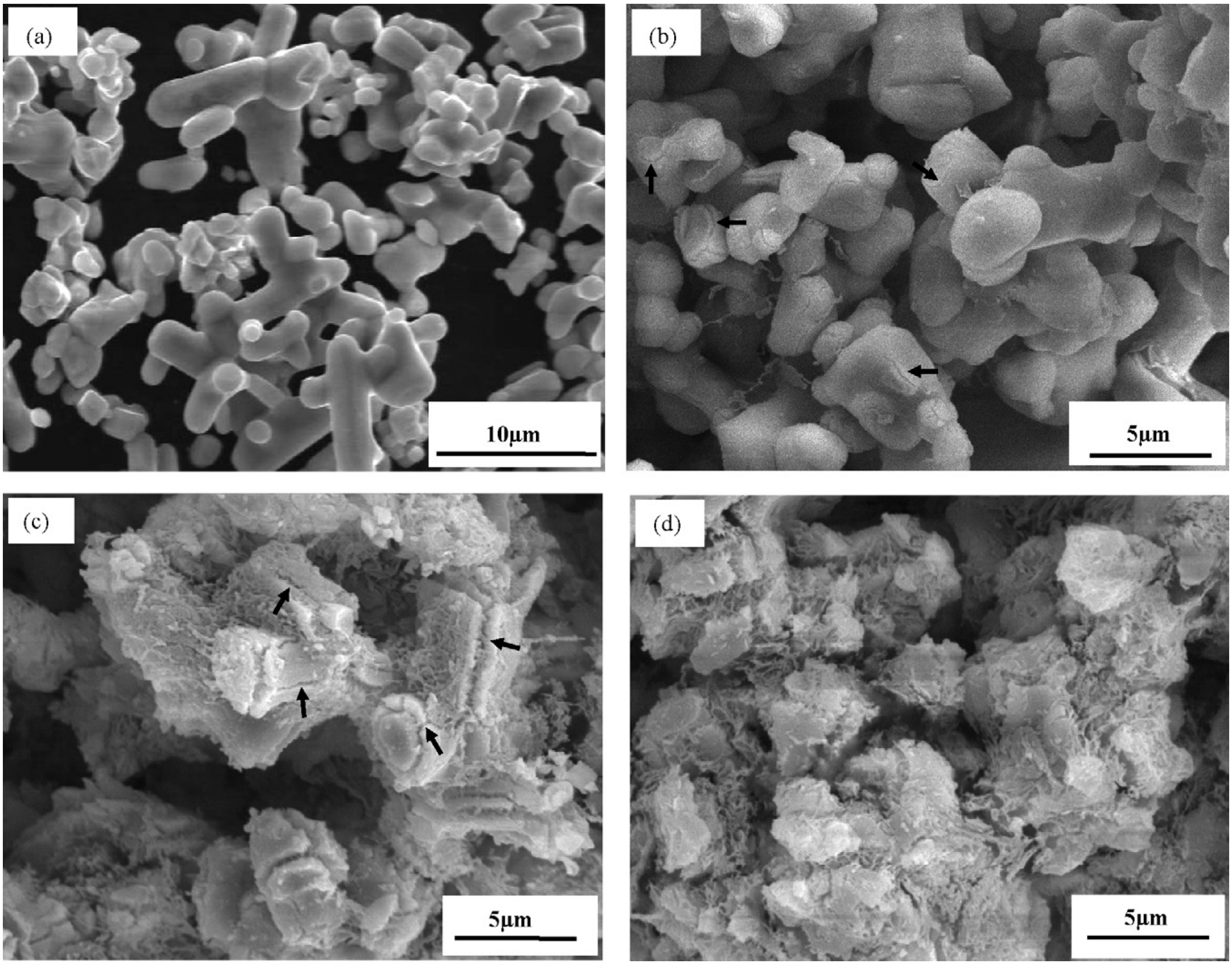

Fig. 5. SEM photographs of ZrB_2 powder oxidized at 700 °C for varying durations: (a) No oxidation; (b) 0.5 h, arrows indicated the microcracks of the ends of columnar particles; (c) 4 h, arrows indicated microcracks of the oxide layers running parallel to the central axes of columnar particles; and (d) 15 h.

6.10 g/cm^3 for ZrB_2 and tetragonal ZrO_2, respectively. In addition, the tetragonal-to-monoclinic phase transformation is accompanied by 5% volume expansion [17]. It is thus understandable that oxidation of ZrB_2 powder is associated with the generation of surface microcracks. Compared with a flat surface, greater stresses induced by volume expansion exist in the edges of columnar ZrB_2 particles. Therefore, microcracks firstly emerge at these edges. With the progress of oxidation, the volume expansion which develops in the oxide layer increases and eventually breaks the particles into fragments.

4. Conclusions

The oxidation of ZrB_2 powder follows para-linear kinetics in air at 650–800 °C, where the dominating term is the parabolic one, accounting for oxygen diffusion in the oxide scale. From 650 to 700 °C, the linear term is positive, which is related to mass gain due to chemical reaction between ZrB_2 and O_2 at the diboride–oxide interfaces. From 750 to 800 °C, the linear term is negative, accounting for mass loss due to vaporization of B_2O_3. Therefore, even though the vapor pressure of B_2O_3 is low in the in the range of 750–800 °C, the effect of evaporation of B_2O_3 should not be neglected during the oxidation of ZrB_2 powder. The reaction product of ZrB_2 powder with oxygen is metastable tetragonal ZrO_2 at 700 °C, and the tetragonal phase transforms to the monoclinic phase with oxidation. The oxidation of ZrB_2 powder is associated with surface microcrack formation, which can be attributed to volume expansion resulting from oxidation of ZrB_2 to tetragonal ZrO_2 and tetragonal-to-monoclinic phase transformation of ZrO_2. Finally, in the last stage of oxidation, each particle breaks into fragments.

Acknowledgement

Financial support from the Chinese Academy of Sciences under the Program for Recruiting Outstanding Overseas Chinese (Hundred Talents Program), the National Natural Science Foundation of China (No. 50632070 and No. 50602048) is gratefully appreciated.

References

[1] A.L. Chamberlain, W.G. Fahrenholtz, G.E. Hilmas, J. Am. Ceram. Soc. 89 (2006) 450–456.
[2] F. Monteverde, A. Bellosi, S. Guicciardi, J. Eur. Ceram. Soc. 22 (2002) 279–288.
[3] A.K. Kuriakose, J.L. Margrave, J. Electrochem. Soc. 111 (1964) 827–831.
[4] W.C. Tripp, H.C. Graham, J. Electrochem. Soc. 118 (1971) 1195–1199.
[5] J.B. Berkowitz-Mattuck, J. Electrochem. Soc. 113 (1966) 908–914.
[6] R.J. Irving, I.G. Worsley, J. Less-Common Met. 16 (1968) 103–112.
[7] F. Monteverde, A. Bellosi, J. Electrochem. Soc. 150 (2003) B552–B559.
[8] D. Sciti, M. Brach, A. Bellosi, Scripta Mater. 53 (2005) 1297–1302.

[9] A. Rezaie, W.G. Fahrenholtz, G.E. Hilmas, J. Am. Ceram. Soc. 89 (2006) 3240–3245.
[10] W.G. Fahrenholtz, J. Am. Ceram. Soc. 90 (2007) 143–148.
[11] A. Rezaie, W.G. Fahrenholtz, G.E. Hilmas, J. Eur. Ceram. Soc. 27 (2007) 2495–2501.
[12] T.A. Parthasarathy, R.A. Rapp, M. Opeka, R.J. Kerans, Acta Mater. 55 (2007) 5999–6010.
[13] K.G. Nickel, in: K.G. Nickel (Ed.), Corrosion of Advanced Ceramics, Kluwer Academic Publishers, Dordrecht, NL, 1994, pp. 59–72.
[14] M. Brach, D. Sciti, A. Balbo, A. bellosi, J. Eur. Ceram. Soc. 25 (2005) 1771–1780.
[15] N. Igawa, T. Nagaski, Y. Ishii, K. Noda, H. Ohno, Y. Morii, J.A. Fernandez-Baca, J. Mater. Sci. 33 (1998) 4747–4758.
[16] X.M. Liu, Z.F. Yan, Chin. J. Struct. Chem. 25 (2006) 424–432.
[17] S. Shukla, S. Seal, Int. Mater. Rev. 50 (2005) 45–64.